Cancer Nanotechnology

RESEARCH Open Access

Black TiO_2-based nanoparticles as Toll-like receptor stimulator delivery system for enhanced photothermal-immunotherapy of pancreatic cancer

Liu Xu[1†], Ruoyu Wu[1,2†], Jiajing Ni[1,2†], Lufei Jin[2], Kaiwei Xu[2], Yuchao Zhu[1], Lu Hong[2], Chunqu Chen[1,2], Linwei Wang[1,2], Lubin Zhu[1,2], Weijian Zhou[1,2], Wenqi Shen[1,2] and Jianhua Wang[3*]

†Liu Xu, Ruoyu Wu and Jiajing Ni have contribute equally to this work.

*Correspondence: wangjianhua@nbu.edu.cn

[1] Department of Radiology, The First Affiliated Hospital of Ningbo University, Ningbo 315010, China
[2] Health Science Center, Ningbo University, Ningbo 315211, China
[3] Department of Radiology, The First Affiliated Hospital of Xiamen University, 55 Zhenhai Road, Xiamen 361000, Siming, China

Abstract

Background: The tumor-specific immune responses, essential for removing residual lesions and preventing tumor metastases, can be stimulated by tumor-associated antigens (TAAs) released following photothermal therapy (PTT). However, due to the immunosuppressed microenvironment of pancreatic ductal adenocarcinoma (PDAC), the TAAs released by PTT are difficult to induce an effective immune response. In this work, we prepared the mesoporous silica ($mSiO_2$) coated black titanium dioxide ($bTiO_2$) photothermal nanoparticles (NPs) for enhanced photothermal-immunotherapy toward PDAC, in which resiquimod (R848) was loaded and DOTA-Gd was conjugated. The NPs are specified as $bTiO_2$@$mSiO_2$@Gd/R848 and abbreviated to NPs/R848. R848 as a kind of Toll-like receptor 7/8 agonist can remodel the tumor microenvironment (TME) in PDAC and induce a strong immune response. Furthermore, DOTA-Gd serves as a magnetic resonance imaging (MRI) contrast agent to improve the T_1-weighted MRI performance of the NPs.

Results: In vitro results of this study show that NPs/R848 could thermally ablate tumor cells and efficiently trigger dendritic cell (DC) maturation. The results of in vivo investigations demonstrate that the combined use of photothermal-immunotherapy exhibits a significant inhibitory effect on tumor growth. Besides, it promoted maturation of DCs and enhanced infiltration of CD8 + , CD4 + T cells to improve the TME in PDAC.

Conclusions: Our study anticipates that by encouraging the maturation of DCs, this strategy will improve the TME and enable the successful photothermal-immunotherapy of PDAC.

Keywords: Pancreatic ductal adenocarcinoma, Nanoparticles, Photothermal-immunotherapy, Toll-like receptor 7/8 agonist

Introduction

Pancreatic ductal adenocarcinoma (PDAC) is currently ranked as the seventh most prevalent cause of cancer-related mortality globally. Unfortunately, the current five-year survival rate for this particular disease remains below 10%, and its incidence is steadily increasing year by year (Siegel et al. 2022; Sung et al. 2021; Rawla et al. 2019). At present, the primary therapeutic approach for patients diagnosed with PDAC involves surgical excision of the affected region, followed by adjuvant radiotherapy and chemotherapy. However, this method is frequently considered unsatisfactory in its treatment outcomes (Neoptolemos et al. 2018; Vincent et al. 2011).

The utilization of nanoparticles (NPs) with a significant photothermal conversion efficiency in the field of photothermal therapy (PTT), to eliminate malignant cells and induce immunogenic cell death (ICD), has garnered considerable interest in the past few decades (Balakrishnan et al. 2020; Wang et al. 2019; Duan et al. 2019). However, because of restrictions on heat shock protein and light penetration depth, a single PTT may not be sufficient to completely ablate a tumor, which could lead to metastasis or recurrence (Huang et al. 2021; Han and Choi 2021). Additionally, the immunosuppressed microenvironment of PDAC makes it difficult for released TAAs from PTT to induce an effective immune response (Liu et al. 2022; Nguyen et al. 2012). Immunotherapy is regarded as an additional crucial cancer treatment method because it stimulates the immune system to combat malignancies. Current immunotherapeutic approaches for cancer encompass a variety of methods such as specific immunomodulators, immune checkpoint blockade (ICB), cancer vaccines, and therapy with chimeric antigen receptor T cells (Zhang and Zhang 2020a). However, PDAC has distinct biological features that make it difficult to treat with a single immunotherapy, including a lack of blood supply, an immunosuppressed microenvironment, and high pressure for dense fibrous matrix within tumors (Hou et al. 2022; Gao et al. 2019). The results of our earlier investigations have demonstrated that PTT can disrupt the fibrous matrix of PDAC models, thereby enhancing the permeability of blood vessels and facilitating improved penetration of therapeutic drugs (Xu et al. 2022). It is challenging to induce an effective immune response with the TAAs generated by PTT in the immunosuppressed microenvironment of PDAC. DCs, as the major antigen-presenting cells (APCs), can induce the formation of specific cytotoxic T lymphocytes (CTLs). Due to their immaturity and low vitality, DCs in the PDAC microenvironment are unable to deliver tumor antigens to effector T cells and initiate an immune response against the tumor (Muller et al. 2022). Immune adjuvants, as non-specific immune enhancers, can function through the following mechanisms: (1) promoting antigen recognition; (2) activating DCs and macrophages; (3) inducing cytokine production (Lee and Suresh 2022). R848 is a Toll-like receptor 7/8 agonist that is recognized by ligands in antigen-presenting intracellular bodies. Its function is to stimulate intracellular signaling pathways that facilitate the maturation of DCs, resulting in the secretion of chemokines and pro-inflammatory cytokines. Effective humoral and cellular immune responses are also induced by its activation of effector T cells. Recent evidence suggests that it remodels the TME and induces a strong immune response in PDAC, leading to increased survival and reduced cachexia in murine models of PDAC (Michaelis et al. 2019; Kim et al. 2019). Significant treatment

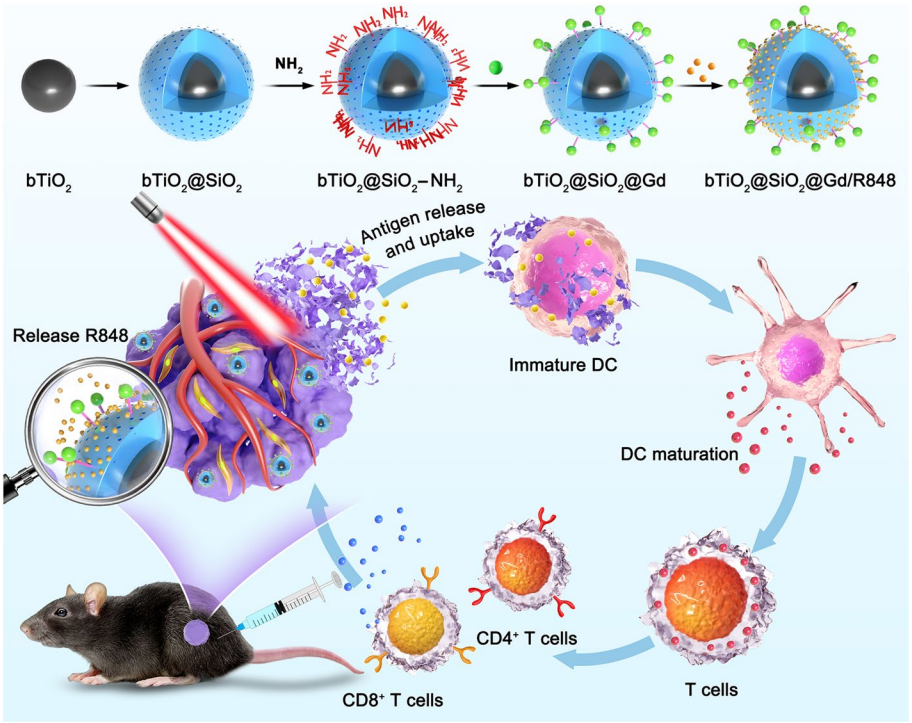

Scheme 1 The synthesis of $bTiO_2$@$mSiO_2$@Gd/R848 NPs and mechanism of $bTiO_2$@$mSiO_2$@Gd/R848 for enhanced photothermal-immunotherapy of pancreatic cancer

outcomes for malignancies have been observed when photodynamic therapy, immunotherapy or chemotherapy were combined with PTT (Xu et al. 2022; Li et al. 2019; Zhou et al. 2018a, b). Hence, the synergistic effect of PTT and the immune adjuvant R848 could increase the rate of antitumor response and impede tumor growth even further.

As a result of advancements in nanotechnology, a variety of NPs with therapeutic visualization capabilities have been designed and implemented in positron emission tomography, computed tomography, ultrasonic imaging, and MRI, among others (Zhang et al. 2020b; Kim et al. 2017; Salvanou et al. 2022). NPs with visual capabilities can observe the absorption, distribution, metabolism, and excretion processes of NPs within the human body in real-time. Furthermore, these NPs can even facilitate the observation of changes in metastasis and tumor growth, enabling the evaluation of the efficacy of tumor treatment (Wang et al. 2022; Zhang et al. 2022). The integration of diagnosis and treatment under the precision medicine model has been further advanced with the advent of visual NPs.

Here, as illustrated in Scheme 1, $bTiO_2$ NPs with good photothermal characteristics were employed as the core; they were then loaded with an agonist (R848) and conjugated with an MRI contrast agent (DOTA-Gd) after being coated with $mSiO_2$ to provide drug-loading sites. The NPs exhibited thermally ablate tumor cells and stimulated the release of TAAs via PTT. Toll-like receptor 7/8 agonist R848 enhanced the immunosuppressive microenvironment of the tumor, promoted the maturation of DCs to enhance the efficacy of TAAs presentation, and stimulated T cell activation

to induce an antitumor immune response. Meanwhile, DOTA-Gd has facilitated the acquisition of T_1-weighted MRI capabilities by the NPs, enabling the visualization of photothermal-immunotherapy for PDAC.

Materials and methods

Reagents

TiO_2 NPs, tetraethyl orthosilicate (TEOS), sodium borohydride ($NaBH_4$), hexadecyltrimethylammonium bromide (CTAB), cyclohexane (C_6H_{12}), concentrated hydrochloric acid (HCl), sodium hydroxide (NaOH), ethanol (C_2H_5OH), 3-(4,5-di-methylthiazol-2-yl)-2,5-diphenyltetrazolium bromide (MTT), Rhodamine B ($C_{28}H_{31}C_lN_2O_3$) and dimethyl sulfoxide (DMSO) were acquired from Aladdin Industrial Inc. (Shanghai, China). The mono-N-hydroxysuccinimide ester (DOTA-NHS Ester) was supplied by Yare Bio Co., Ltd (Shanghai, China). Macklin Biochemical Co., Ltd (Shanghai, China) provided the 3-aminopropyltriethoxysilane (APTES) and gadolinium acetate hydrate ($C_6H_{11}GdO_7$). Fetal bovine serum (FBS), DMEM medium, RPMI-1064 medium and Trypsin–EDTA 0.25% were obtained from Gibco (Grand Island, USA). The phosphate buffer saline (PBS) and penicillin—streptomycin solutions were acquired from GE Healthcare HyClone (LA, USA). Solarbio Biotech Co., Ltd. (Beijing, China) supplied both formaldehyde solution and Hoechst 33,258 ($C_{25}H_{24}N_6O{\cdot}3HCl$). Beyotime Biotech Co., Ltd (Shanghai, China) provided the calcein-AM/PI double stain kit. Resiquimod (R848) was obtained from InvivoGen (San Diego, CA, USA). Binding buffer was purchased from Immunostep (Salamanca, Spain).

Synthesis of $mSiO_2$-coated $bTiO_2$-based nanoparticles

Synthesis of $bTiO_2$ nanoparticles

The TiO_2 was reduced to $bTiO_2$ employing $NaBH_4$ as the reducing agent. Initially, 1 g of TiO_2 powder was mixed with $NaBH_4$ at a 1:1 mass ratio for 30 min before being placed in a tube furnace heated with 10 °C min^{-1}. Under an argon atmosphere, the temperature was raised to 350 °C, and the reaction lasted for 3 h. The produced $bTiO_2$ NPs were washed with ultrapure water, centrifuged thrice to eliminate $NaBH_4$, and then dried for further use.

Synthesis of $bTiO_2$@$mSiO_2$ nanoparticles

Ultrasound was employed to disperse 100 mg of $bTiO_2$ NPs in 20 mL of water. 0.3 mL of 0.1 mM NaOH solution and 500 mg of CTAB were added to the $bTiO_2$ solution, which was then heated to 60 ℃ with magnetic stirring. 20 mL of cyclohexane containing TEOS (20 V/V%) was added after 2 h of magnetic stirring, and the mixture was then continuously stirred at 60 ℃ for 24 h. CTAB was removed from $mSiO_2$-coated $bTiO_2$ by heating it to 80 °C in acetone following centrifugation and alternating washings with ethanol and water. Centrifugation was then employed to collect the as-prepared $bTiO_2$@$mSiO_2$ NPs.

Synthesis of DOTA-Gd-modified $bTiO_2$@$mSiO_2$

The surface of $bTiO_2$@$mSiO_2$ was amino-functionalized by APTES. In particular, 20 mg $bTiO_2$@$mSiO_2$ NPs was dispersed in 20 mL of ethanol, followed by the addition of 2 mL of APTES and heating to 80 ℃ while stirring for 12 h. After centrifugation, the prepared

$bTiO_2$@$mSiO_2$-NH_2 NPs were collected and subjected to modification using gadolinium acetate hydrate and DOTA-NHS-Ester. The PH value of the gadolinium acetate hexahydrate solution was adjusted to 6.5 by adding NaOH after an excessive quantity of DOTA-NHS-ester was introduced. Following a 24-h stirring period, the dispersion of $bTiO_2$@$mSiO_2$-NH_2 was introduced into the reaction system. The pH value was subsequently adjusted to a range of 7.5–8.5, and the mixture was stirred for an additional 24 h at ambient temperature. The DOTA-Gd-modified $bTiO_2$@$mSiO_2$@Gd NPs were obtained after centrifugation.

Synthesis of $bTiO_2$@$mSiO_2$@Gd/R848 nanoparticles

R848 was loaded by physical adsorption. Briefly, $bTiO_2$@$mSiO_2$@Gd and R848 were mixed in sterile water at a mass ratio of 1:10. After stirring for 24 h, the $bTiO_2$@$mSiO_2$@Gd/R848 NPs were obtained by centrifugation.

Characterization

Transmission electron microscopy (TEM, FEI Tecnai F20) was utilized to examine the micro-morphologies of NPs. The zeta potential and hydrated particle size distribution of the NPs were determined using a nano-size zeta potential analyzer (Nano ZS, Malvern Instruments Ltd, England). The UV—visible absorption spectra of the NPs were examined using a UV—visible spectrophotometer (T10CS, Persee General Equipment Co., Ltd, China). The Fourier transform infrared spectrometer (FTIR, Thermo Nicolet 6700, US) was employed to acquire the infrared (IR) spectra of the NPs. The elemental composition was examined using an inductively coupled plasma optical emission spectrometry (ICP-OES) system developed by Spectro Analytical Instruments GmbH of Germany. MR scanners were utilized to examine the relaxation and MRI characteristics of NPs. Furthermore, to assess the photothermal performance of $bTiO_2$@$mSiO_2$@Gd/R848 NPs, cuvettes were filled with 1 mL of $bTiO_2$@$mSiO_2$@Gd/R848 dispersions with varying concentrations of Ti (0–200 μg mL^{-1}) and exposed to 808 nm near-infrared (NIR) radiation for 600 s at 1.5 W cm^{-2}. To determine the power-dependent photothermal performance in the NIR, 1 mL of $bTiO_2$@$mSiO_2$@Gd/R848 dispersions containing 150 μg mL^{-1} Ti were exposed to an 808 nm NIR for 600 s at different power densities (0.5–2.0 W cm^{-2}). To assess photothermal stability, 6 on/off repeating cycles of 808 nm NIR (1.5 W cm^{-2}) were applied to 1 mL of $bTiO_2$@$mSiO_2$@Gd/R848 every 300 s. The imaging acquired through the use of the IR thermal imaging equipment was compiled for subsequent comparisons, and the temperature values continually collected were analyzed and represented as time—temperature curves.

Cytotoxicity of the nanoparticles

To examine the cytotoxicity of $bTiO_2$@$mSiO_2$@Gd/R848 and $bTiO_2$@$mSiO_2$@Gd NPs, Panc02 cells were cultured for 24 h in 96-well plates after seeding. After removing the old culture medium, various amounts of NPs (50–300 μg mL^{-1} of Ti) were introduced to each well and left to incubate for 24 h in the incubator. Following that, MTT reagent (20 μL; 5 mg mL^{-1} in PBS) was introduced to each well and left for another 4 h. After removing the mediums, DMSO was employed to dissolve the formazan crystals. Cell

viabilities were calculated by detecting the absorbance of formazan solutions using the microplate absorbance reader.

Characterization of cellular uptake

The uptake of $bTiO_2$@$mSiO_2$@Gd/R848 NPs by Panc02 cells was observed by fluorescence confocal microscopy. Rhodamine B, a fluorescent dye, was utilized to label the $bTiO_2$@$mSiO_2$@Gd/R848 NPs. Panc02 cells were cultivated with DMEM or $bTiO_2$@$mSiO_2$@Gd NPs (150 μg mL^{-1} of Ti) in a 35 mm Petri dish for 4, 8, and 12 h, respectively. Before being fixed in 4% paraformaldehyde, the cells were washed twice in PBS. After that, the cells were washed with PBS and then treated with Hoechst 33342 (2 μg mL^{-1}) to stain the nucleus.

In vitro PTT evaluation

Panc02 cells were cultured for 12 h in 96-well plates with DMEM, $bTiO_2$@$mSiO_2$@Gd or $bTiO_2$@$mSiO_2$@Gd/R848 NPs (150 μg mL^{-1} of Ti). The media were subsequently substituted with fresh DMEM. The 808 nm NIR laser was delivered by an optical fiber delivery system with a diffusion micro-lens to deliver uniform laser distribution over the cell culture area. Each well was exposed to an 808 nm NIR laser for 5 or 10 min at 0.5, 1.0, or 1.5 W cm^{-2} power densities, respectively. Cell viability was then evaluated using MTT. In addition, the CAM/PI staining approach was utilized to directly evaluate the cell state following therapy. Panc02 cells were specifically exposed to 808 nm NIR (1.5 W cm^{-2}) radiation for 0, 5 or 10 min after being cultured for 12 h in DMEM or $bTiO_2$@$mSiO_2$@Gd/R848 NPs (150 μg mL^{-1} of Ti). The cells were then examined using fluorescence microscopy after being stained with CAM/PI.

PTT synergistic immunotherapy promotes DC maturation in vitro

The transwell method was implemented as a means to examine the impact of NPs on the in vitro maturation of DCs. The upper section included Panc02 cells after various treatments, while the lower section contained DCs. The various treatments were as follows: following incubation with DMEM, $bTiO_2$@$mSiO_2$@Gd NPs, or $bTiO_2$@$mSiO_2$@Gd/R848 NPs (150 μg mL^{-1} of Ti), the Panc02 cells were irradiated with or without 808 nm NIR (1.5 W cm^{-2}), respectively. The mode of 808 nm NIR laser is the same as before, and the exposure duration was 5 min. Each cell was cultured for an additional 32 h. After collecting and staining DCs in the lower chamber with CD11c, CD86 and CD80, flow cytometry was employed to examine the expression of co-stimulatory molecules CD86 and CD80 on DCs in various treatment groups.

In vivo toxicity evaluation of nanoparticles

Female C57BL/6 mice (6 − 8 weeks) were randomly divided into three groups to assess the in vivo toxicity of the NPs. The mice were administered intravenous injections of PBS, $bTiO_2$@$mSiO_2$@Gd or $bTiO_2$@$mSiO_2$@Gd/R848, and their weights were then measured during a feeding period of 20 days. The dose of nanoparticles was 20 mg kg^{-1}. After 20 days, all mice were killed. Routine blood tests were performed on the mice in each group, and their major organs, such as the lung, heart, liver and spleen, were fixed

in a 10% formalin solution and histologically examined using hematoxylin and eosin (H&E) staining.

In vivo MR evaluation

The mice were subcutaneously injected with 1×10^6 Panc02 cells in the right flank of the mice to establish the PDAC models. Both PBS and NPs/R848 were administered intratumorally to the mice. The MR images of the tumors were captured by a 3.0 T MRI system (MAGNETOM Prisma, Siemens).

In vivo PTT synergistic immunotherapy

Six groups of female C57BL/6 mice (6–8 weeks) were randomly assigned. To generate the PDAC models, 1×10^6 Panc02 cells were subcutaneously injected in the right flank of the mice. The tumors were then given time to grow until reached 250 mm^3 before experiments. To assess the synergistic immunotherapy of PTT in vivo, subcutaneous tumors were directly irradiated by 808 nm NIR laser above the tumor sites at the power density of 1.5 W cm^{-2} for 5 min. The following treatments were administered to the tumor-injected mice: (1) In the NPs/R848 or NPs/R848 + Laser groups, $bTiO_2$@$mSiO_2$@Gd/R848 was administered, followed by 808 nm NIR laser irradiation or not. (2) The NPs or NPs + Laser groups were given $bTiO_2$@$mSiO_2$@Gd before being exposed to an 808 nm NIR laser or not. (3) The PBS or PBS + Laser group received PBS before being irradiated with an 808 nm NIR laser or not. The dose of NPs/R848 was 4 mg kg^{-1}. The body weights and tumor volumes of various groups were assessed on alternate days over 14 days. Furthermore, the main tumors retrieved from the mice on the third day of treatment were embedded in paraffin wax after being preserved in neutral buffered formalin (10%). Subsequently, the embedded tissue samples underwent sectioning and were subjected to blocking using a 2.5% Normal Goat Serum Blocking Solution. Following this, the samples were stained with H&E, CD80, CD86, CD4, and CD8.

Statistical analysis

Data were presented as mean ± standard deviation and compared using the Student's t–test. $P < 0.05$ was set as the significance level.

Results

Characterization of as-prepared nanoparticles

Scheme 1 depicts the synthesis of $bTiO_2$@$mSiO_2$@Gd/R848 NPs. To improve drug loading efficiency, core—shell nanocomposites were formed by coating $bTiO_2$ NPs with $mSiO_2$. In addition, gadolinium (Gd) was subsequently used to integrate the MRI function with the nanoparticles. The DOTA-NHS-Ester reagent was attributed to conjugate amino groups through the NHS-ester and chelate Gd^{3+} ion by DOTA (Wang et al. 2018). Finally, R848 was loaded on NPs by physical adsorption. TEM analysis revealed the morphological characteristics of $bTiO_2$@$mSiO_2$@Gd and $bTiO_2$@$mSiO_2$@Gd/R848 NPs (Fig. 1a–b), respectively. According to the TEM analysis, the average size of the $bTiO_2$@$mSiO_2$@Gd/R848 NPs was around 149.8 nm. According to Fig. 1c, which displays the FTIR spectra of several samples, $bTiO_2$@$mSiO_2$@Gd exhibited peak shifts at C = O (1576 cm^{-1}) and C–N (1483 cm^{-1}), suggesting that

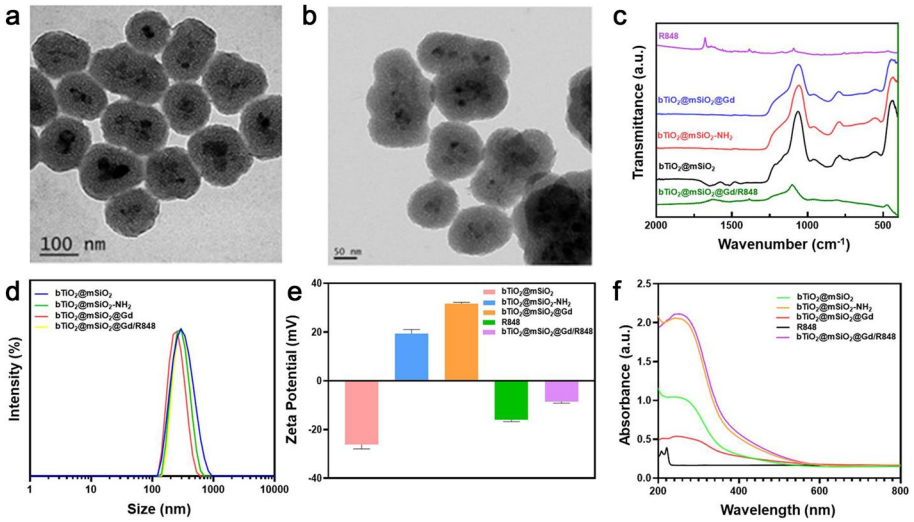

Fig. 1 Characterization of the chemical and physical properties of NPs. TEM images of (**a**) $bTiO_2@mSiO_2@Gd$ and (**b**) $bTiO_2@mSiO_2@Gd/R848$ at different magnifications. **c** FTIR spectra, d particle sizes, **e** zeta potentials, and (**f**) UV—visible spectra of the NPs

an amide reaction took place between $bTiO_2@mSiO_2$-NH_2 and DOTA-Gd, leading to the successful connection of DOTA-Gd. The FTIR spectrum of $bTiO_2@mSiO_2@Gd/R848$ changed significantly in comparison to $bTiO_2@mSiO_2@Gd$, this change was ascribed to the loading of R848. The mean hydrated sizes of $bTiO_2@mSiO_2$, $bTiO_2@mSiO_2$-NH_2, $bTiO_2@mSiO_2@Gd$, and $bTiO_2@mSiO_2@Gd/R848$ were approximately 191.3 nm, 240.7 nm, 288.9 nm, 290.5 nm, respectively (Fig. 1d). The results indicate that particle sizes gradually increase with the modification of related components. In addition, the zeta potentials of R848, $bTiO_2@mSiO_2$, $bTiO_2@mSiO_2$-NH_2, $bTiO_2@mSiO_2@Gd$ and $bTiO_2@mSiO_2@Gd/R848$ were about −16 mV, −26.2 mV, 19.4 mV, 31.7 mV, −8.5 mV, respectively (Fig. 1e). The surface charge of $bTiO_2@mSiO_2@Gd$ exhibited a reduction from 31.7 to −8.5 mV after the introduction of agonist R848 as determined by the DLS. R848 is successfully loaded onto $bTiO_2@mSiO_2@Gd$, as evidenced by the partial neutralization of its positive charge by the negative charge of R848. The $bTiO_2@mSiO_2@Gd/R848$ with negative surface charge prolongs blood circulation and efficiently accumulates into tumor tissues through enhanced permeability and retention effect, making it potentially useful for in vivo studies (Zhang et al. 2022). As shown in the UV—visible spectra of various samples, there was no substantial change in the absorption peak of $bTiO_2@mSiO_2@Gd/R848$ (Fig. 1f).

MR and photothermal performance properties

The MR characteristics of NPs were assessed utilizing a 0.5 T MR scanner system. Magnevist, a commercial contrast agent, was utilized as the control. Figure 2a, b shows that at the same dose of Gd, the r_1 values for $bTiO_2@mSiO_2@Gd/R848$ and Magnevist were 6.623 and 4.099 mM^{-1} s^{-1}, respectively. The corresponding values for r_2 were 7.772 mM^{-1} s^{-1} and 4.284 mM^{-1} s^{-1}, respectively. The r_2/r_1 ratio of $bTiO_2@mSiO_2@Gd/R848$ is around 1.17, suggesting that the NPs exhibit potential as MRI contrast agents

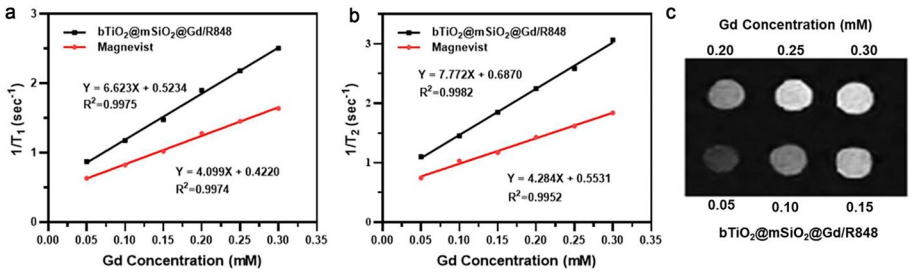

Fig. 2 The MR characteristics of NPs. The fitted relaxation ($1/T_1$ and $1/T_2$) plots of $bTiO_2$@$mSiO_2$@Gd/R848 and Magnevist, **a** longitudinal, and (**b**) transverse with an equivalent concentration of Gd. **c** T_1-weighted MR imaging of $bTiO_2$@$mSiO_2$@Gd/R848 at various Gd concentrations

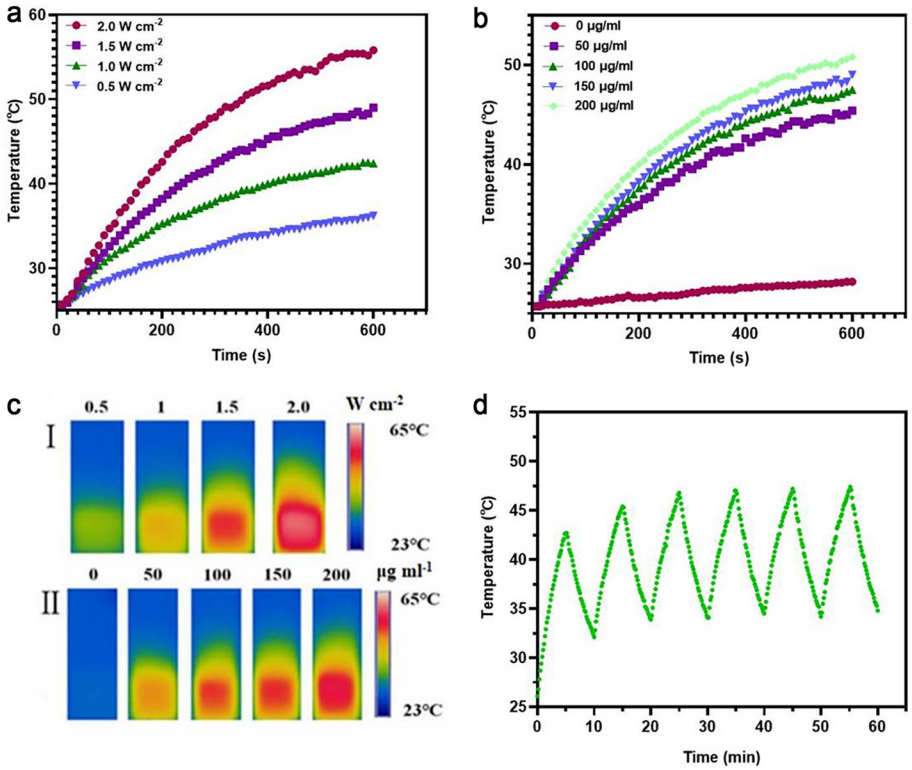

Fig. 3 The temperature curves of $bTiO_2$@$mSiO_2$@Gd/R848 at (**a**) different power densities and (**b**) various concentrations. **c** Typical pictures of thermal imaging. **d** Temperature profile of $bTiO_2$@$mSiO_2$@Gd/R848 during 6 on/off cycles when illuminated with an 808 nm NIR laser

due to their superior T_1-weighted contrast efficacy ($r_2/r_1 < 3$) (Guo et al. 2017). Figure 2c displays the T_1-weighted MR imaging of $bTiO_2$@$mSiO_2$@Gd/R848.

Previous studies have demonstrated that $bTiO_2$ NPs exhibit a significant photothermal capability (Wang et al. 2018). The PTT performance of the $bTiO_2$@$mSiO_2$@Gd/R848 NPs that were synthesized by modifying $bTiO_2$ NPs with silicon oxide was assessed in this investigation. After being exposed to an 808 nm NIR laser for 10 min at various power densities, the temperatures of 1 mL $bTiO_2$@$mSiO_2$@Gd/R848 dispersions rapidly increase, as illustrated in Fig. 3a. As the 808 nm NIR power density increased, there was a corresponding acceleration in the rise of dispersion

temperature. Following a 10-min exposure to 1.5 W cm^{-2} of 808 nm NIR radiation, the temperature of 1 mL $bTiO_2$@$mSiO_2$@Gd/R848 dispersions increased to around 50 ℃. Within minutes of exposure, tumor cells can experience fast ablation at this temperature (Qi et al. 2019). Subsequently, the dispersions were exposed to 1.5 W cm^{-2} of 808 nm NIR radiation at various concentrations, varying from 0 to 200 μg mL^{-1}. As depicted in Fig. 3b, an increase in the concentration of Ti in dispersions leads to a more rapid rise in the temperature of the dispersions. The temperature curves in Fig. 3a, b are consistent with the real-time photothermal images shown in Fig. 3c I, II. The photothermal stability of NPs is also very important. As shown in Fig. 3d, $bTiO_2$@$mSiO_2$@Gd/R848 were exposed to on/off cycles of 808 nm NIR (1.5 W cm^{-2}) every 5 min for 1 h. Throughout the irradiation cycle, the temperature curve for heating and cooling remained constant, indicating that $bTiO_2$@$mSiO_2$@Gd/R848 NPs are stable when exposed to NIR radiation.

Cell uptake of nanoparticles

The uptake and internalization of NPs by tumor cells are crucial for cancer therapy. The cell nucleus stained with Hoechst 33342 in blue and Rhodamine B-labeled NPs in red were observed by fluorescence confocal microscopy. The increase in co-incubation time resulted in a corresponding increase in cellular absorption of NPs,

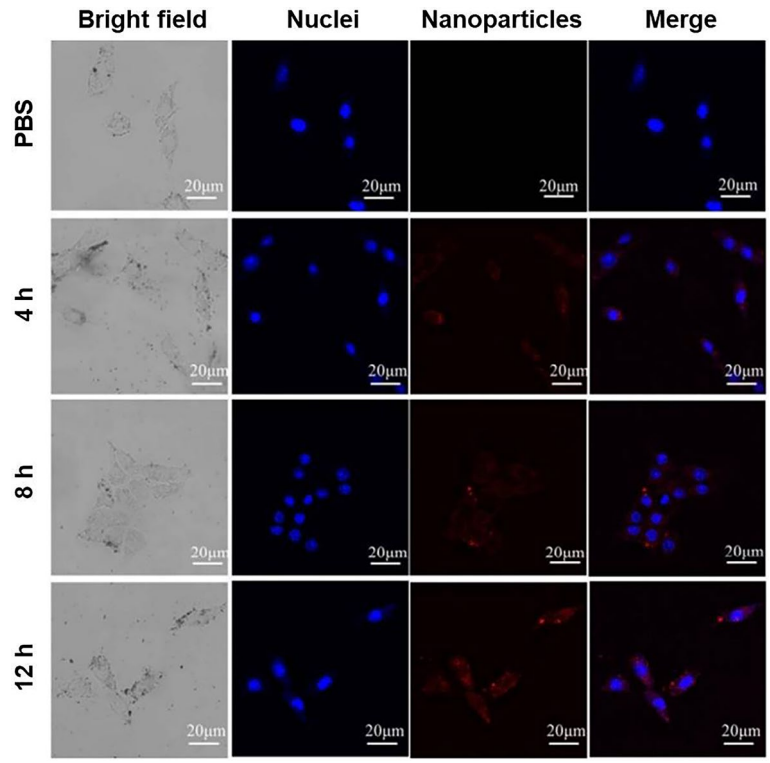

Fig. 4 Confocal fluorescence microscopy images of Panc02 cells incubated with $bTiO_2$@$mSiO_2$@Gd/R848 NPs for 4, 8, and 12 h, respectively. Red fluorescence indicates Rhodamine B-labeled NPs, while blue fluorescence indicates Hoechst 33342-labeled nuclei. (scale bar: 20 μm)

as illustrated in Fig. 4. The findings suggest that Panc02 cells can internalize $bTiO_2$@$mSiO_2$@Gd/R848 NPs and after 12 h, there were enough nanoparticles swallowed by the cells, which could be followed by PTT.

Cytotoxicity assay

Although earlier research has established the reduced toxicity of $bTiO_2$ NPs in both in vitro and in vivo settings (Xu et al. 2022), it is important to note that the inclusion of CTAB as a template during nanocomposite synthesis and the loading of R848 further necessitates an evaluation of the cytotoxicity of $bTiO_2$@$mSiO_2$@Gd/R848 NPs. The cytotoxic effects of $bTiO_2$@$mSiO_2$@Gd and $bTiO_2$@$mSiO_2$@Gd/R848 on Panc02 cells are illustrated in Fig. 5a. After incubation for 24 h, more than 80% of the cells were viable for NPs containing Ti concentrations between 50 and 300 μg mL^{-1}, indicating that the NPs have minimal cytotoxicity and can be applied in biotherapy.

PTT performance of pancreatic *cancer* in vitro

The systematic evaluation of the PTT efficacy of the NPs in vitro was conducted using the MTT assay, as illustrated in Fig. 5b. Before being exposed to 808 nm NIR radiation under various settings, Panc02 cells were maintained in DMEM, $bTiO_2$@$mSiO_2$@Gd (NPs), and $bTiO_2$@$mSiO_2$@Gd/R848 (NPs/R848) for 12 h. Following a 10-min exposure with 808 nm NIR at power density of 1.5 W cm^{-2}, the cell survival rates were 80.1% ± 2.9% for the Laser group, 40.9% ± 4.0% for the NPs group, and 39.7% ± 1.4% for the NPs/R848 group. Tumor cells were effectively photothermally destroyed by both $bTiO_2$@$mSiO_2$@Gd and $bTiO_2$@$mSiO_2$@Gd/R848 NPs, with the substance R848 having no discernible effect on this outcome, according to the results.

Moreover, the live/dead cell staining assay was employed to investigate the PTT performance of NPs on Panc02 cells. As depicted in Fig. 5c, live cells were labeled

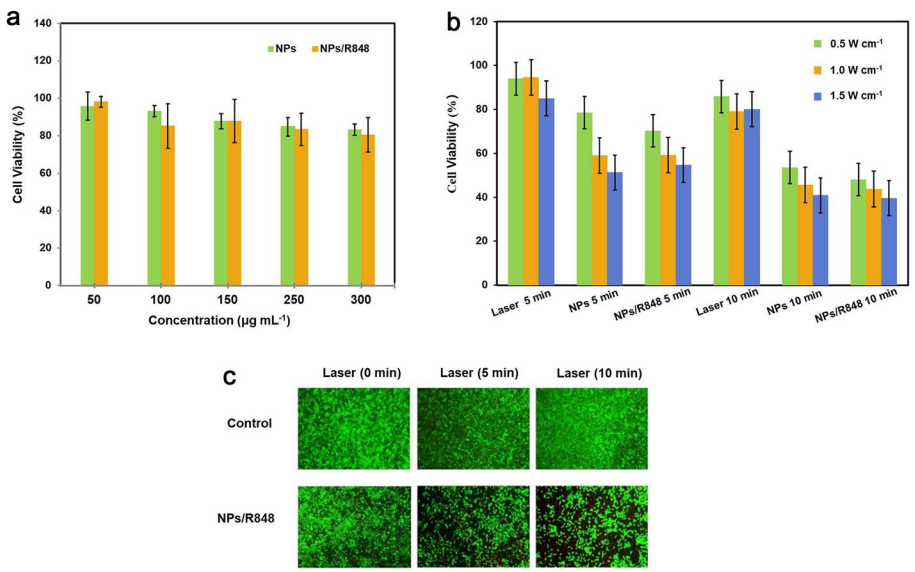

Fig. 5 **a** Cytotoxicity assessment of NPs on Panc02 cells. **b** Study on photothermal ablation impact of NPs on Panc02 cells. **c** Calcein-AM (green) and PI (red)-stained Panc02 cells fluorescence imaging following different treatments (scale bar: 50 μm)

with green fluorescence (Calcein-AM), while dead cells were indicated with red fluorescence (PI). After being exposed to an 808 nm NIR laser, most of the panc02 cells in DMEM survived, however many Panc02 cells in $bTiO_2$@$mSiO_2$@Gd/R848 died. An increase in irradiation duration resulted in a greater destruction of Panc02 cells. The results obtained from the live/dead cell staining are in agreement with the outcomes of the MTT test. The aforementioned findings suggest that $bTiO_2$@$mSiO_2$@Gd/R848 NPs exhibit a strong photothermal killing effect on Panc02 cells.

PTT synergistic immunotherapy promoted DC maturation in vitro

DCs have an essential role as a link between the adaptive and innate immune responses, making them one of the most important APCs. Both naive cytotoxic T cells (CD8 +) and helper T cells (CD4 +) can be activated by mature DCs. To examine the in vitro impact of $bTiO_2$@$mSiO_2$@Gd/R848 NPs on the promotion of DC maturation, the transwell system is implemented. The results presented in Fig. 6 indicate that the maturation of DCs was significantly increased from 17.3% to 48.5% in the NPs/R848 (−) group comparing to the NPs (−) group where R848 was absent. In addition, at the same dose of R848 as the NPs/R848 (−) group, DC maturation in NPs/R848 (+) group increased by 53.4%. Moreover, the maturation of DCs was observed to increase from 0.59% to 17.3% in the NPs (-) group without irradiation, in comparison to the control (−) group. This finding suggests that $bTiO_2$@$mSiO_2$@Gd NPs, in the absence of the R848 drug, also serve as an immune adjuvant and have the ability to stimulate DCs maturation.

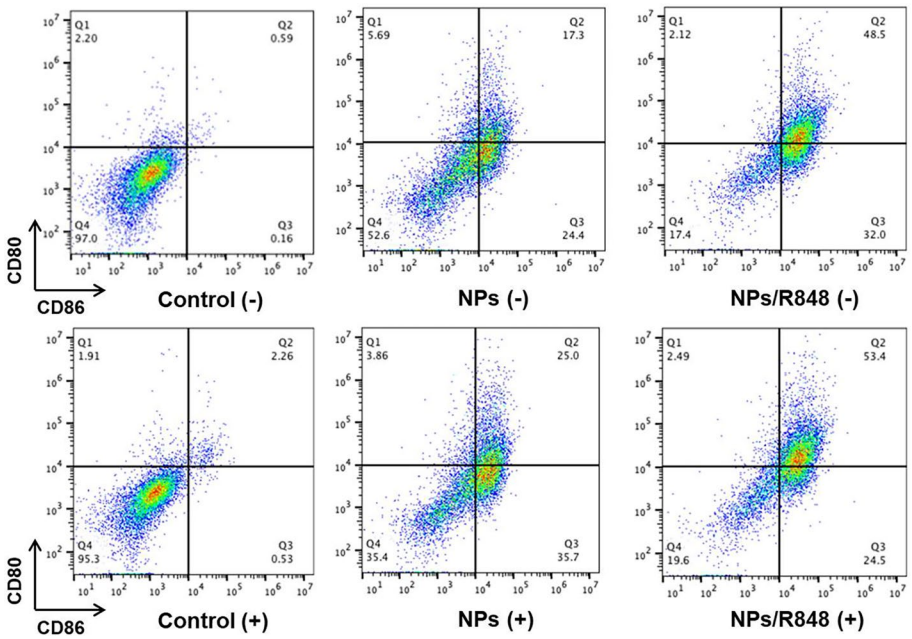

Fig. 6 The investigation of in vitro transwell coculture systems. Panc02 cells are grown in the upper section, while DCs are placed in the lower section. In the coculture system, DCs and Panc02 cells are subjected to various treatments. Following different treatments, the percentage of mature DCs is determined via flow cytometry

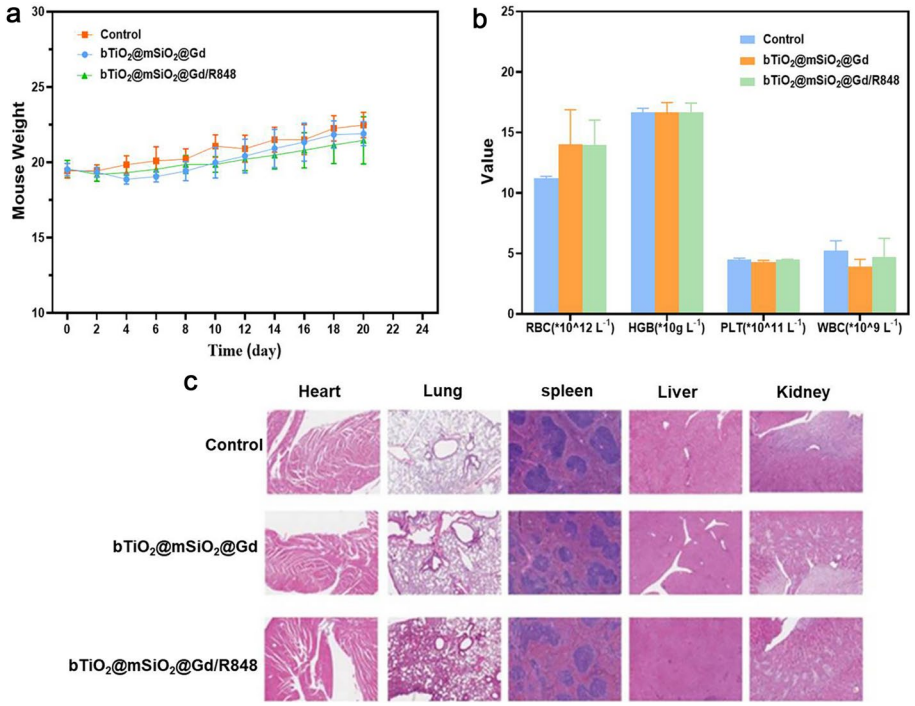

Fig. 7 Toxicity assessment of NPs in vivo. **a** The variation in body weights, **b** routine blood indexes, and (**c**) the staining of major organs (liver, kidney, heart, spleen and lungs) with H&E of mice after being injected with PBS, $bTiO_2$@$mSiO_2$@Gd, and $bTiO_2$@$mSiO_2$@Gd/R848 for 20 days. (scale bar: 100 μm)

In vivo toxicity evaluation of nanoparticles

The body weights, blood routine indicators and organ histology of mice were evaluated to determine the toxicity of the treatments. Following injection, mice in each group were weighed within 20 days (Fig. 7a). Figure 7b, c show the blood routine indexes and histology of the organs after injection for 20 days. There were no appreciable changes in blood routine indicators or significant losses in body weights when compared to the PBS-injected control group. Moreover, the $bTiO_2$@$mSiO_2$@Gd-and $bTiO_2$@$mSiO_2$@Gd/R848-injected groups exhibited no discernible tissue injury or other lesions, including necrosis, inflammation or pulmonary fibrosis. These findings demonstrate that the treatments are safe and well-tolerated in PDAC models.

Photothermal imaging, MRI and PTT synergistic immunotherapy in vivo

Photothermal imaging of $bTiO_2$@$mSiO_2$@Gd/R848 and PBS-injected tumor-bearing mice exposed to 808 nm NIR is presented in Fig. 8a. Compared to the control group of mice that were injected with PBS and exposed to 808 nm NIR radiation, the group that received injections of NPs/R848 showed a significantly rapid increase in tumor site temperature after the injections. Figure 8b illustrates the temperature profile at the sites of tumors when exposed to NIR irradiation. Exposure to temperatures above 50 °C has been reported to cause the ablation of tumor cells within a few minutes (Qi et al. 2019). Previous research indicated that exposing cells to 50 °C effectively killed tumor cells in the NPs/R848 group following NIR irradiation. Figure 8c depicts MRI images of

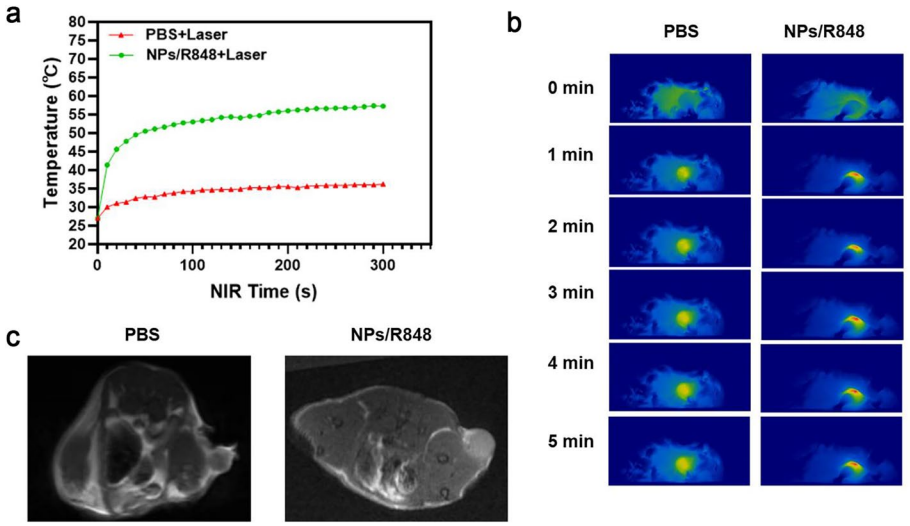

Fig. 8 **a** Tumor temperature alterations and (**b**) photothermal images of the tumors in the PBS and NPs/R848 groups after 5 min of NIR radiation at the power density of 1.5 W cm^{-2}. **c** MRI images of tumors in the PBS and NPs/R848 groups

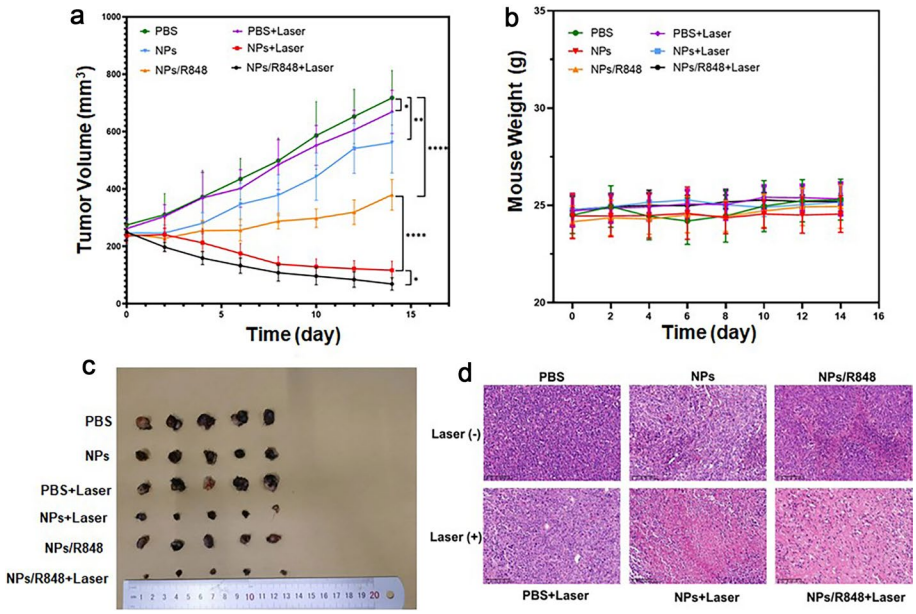

Fig. 9 **a** The tumor volumes and (**b**) the body weights of mice following various treatments. Data are expressed as mean ± standard deviation (n = 5). **c** An image of the tumors taken 14 days after treatment. **d** H&E staining of tumor tissue after treatment. (Scale bar: 100 μm) *p < 0.05, **p < 0.01, ***p < 0.001, ****p < 0.0001 were evaluated via Student's t test

mice from different groups. The intratumoral T_1-weighted MRI of the NPs/R848 group showed a strong signal, confirming that NPs/R848 has T_1-weighted MRI performance, in comparison to the PBS group.

Tumor-injected mice were divided into six groups and treated for 14 days to evaluate PTT synergistic immunotherapy in vivo. Changes in tumor volume after treatment

are illustrated in Fig. 9a. The tumors exhibited a significant increase in growth rate upon treatment with either PBS or PBS combined with NIR irradiation (PBS + Laser). In comparison to the control group (PBS), tumor growth was slightly suppressed in mice treated with $bTiO_2$@$mSiO_2$@Gd (NPs) or $bTiO_2$@$mSiO_2$@Gd/R848 (NPs/R848). However, mice injected with $bTiO_2$@$mSiO_2$@Gd or $bTiO_2$@$mSiO_2$@Gd/R848 and exposed to NIR irradiation (NPs + Laser) or (NPs/R848 + Laser) displayed tumor growth inhibition. Notably, the NPs/R848 + Laser group demonstrated significantly stronger antitumor efficacy because of the combined impact of immunotherapy and PTT. To assess the toxicity of the treatments, the body weight of the mice was measured after 12 days; no statistically significant variations were observed between groups (Fig. 9b), suggesting that the treatments are tolerable and safe for use in PDAC models. Figure 9c depicts tumor images with varying degrees of antitumor activity across different treatment groups. Figure 9d further illustrates the variation in cell damage between these groups. Except for mice that are used to immune analysis, all of the mice survived until some tumors exceed 2000 mm^3 in size and were euthanized.

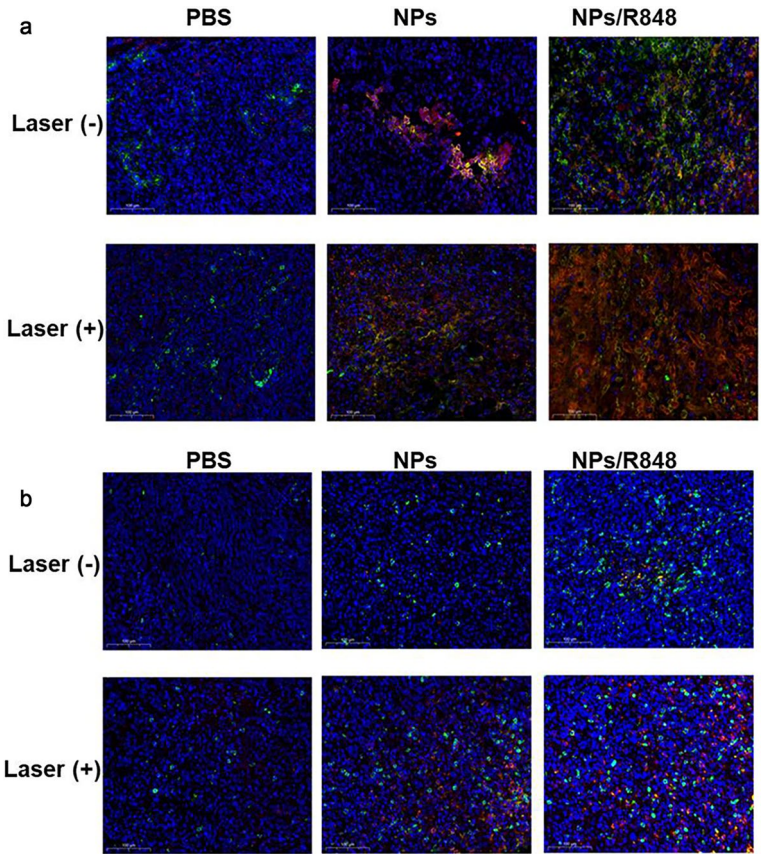

Fig. 10 The immunofluorescence staining of tumor tissues on day 3 after different treatments. **a** Green indicates CD80 and red indicates CD86. **b** Green indicates CD4 and red indicates CD8. (Scale bar: 50 μm)

Immune response in Vivo

In vitro experiments indicate that the Panc02 cells residue post NIR-induced PTT with NPs/R848 significantly accelerates the maturation of DCs in comparison to the other groups. Based on these findings, it appears that NPs/R848 can be used as an adjuvant in photothermal-immunotherapy to stimulate the immune response against cell residues containing TAAs. In further in vivo experiments, the levels of DC maturation were investigated through immunofluorescence staining. In comparison to the other groups, the NPs/R848 + Laser group demonstrated greater DCs maturation (Fig. 10a). This outcome is in line with the flow analysis, which showed that in vitro, the NPs/R848 + Laser group caused higher DCs maturation than the other groups. This indicates that more DCs are drawn to the tumor site as APCs to engulf the TAAs and DAMPs released by apoptotic tumor cells and mature with the aid of released R848. Having the ability to eliminate tumor cells, CD8 + and CD4 + T cells function as the ultimate effector T cells for tumor immunity. The TME causes immunologic tolerance, which in turn causes CTLs to become dysfunctional and exhausted during carcinogenesis. Hence, further immunofluorescence staining was carried out to determine if NPs/R848 altered tumor CTL activation for photothermal-immunotherapy. Figure 10b shows that the NPs/R848 + Laser group had considerably increased levels of CD4 + and CD8 + T cell expression compared to the other groups. This suggests that the combinatorial therapy had a positive effect on CD8 + and CD4 + expression, as well as their associated immune responses, leading to a remarkable improvement in antitumor efficiency. All of these results indicate that this combinatorial therapy effectively promotes DCs maturity and increases the number of CD8 + and CD4 + T cells, stimulates an antitumor immune response, and improves the immunosuppressed microenvironment of PDAC.

Discussion

In this work, we have prepared novel bTiO_2@mSiO_2@Gd/R848 NPs as photothermal-immunotherapy agents for PDAC, which are capable of inducing direct harm to tumor cells via PTT, promoting DC maturation and thereby stimulating T cell-associated immune responses. As evidenced by in vitro tests, this synergistic therapy successfully stimulates DC maturation and destroys tumor cells upon NIR-induced PTT. In vivo results further showed that synergistic therapy activates T cell—associated immune responses to inhibit tumor growth.

PPT is widely used in cancer therapy because of its economical, minimally invasive and highly efficient treatment. A study on the photothermal-immunotherapy of pancreatic cancer by direct laser and GC as immunologic adjuvant has been reported to successfully inhibit tumor growth, recurrence and metastasis (Zhou et al. 2018a, b). However, compared to direct laser, due to the high permeability and retention effect of solid tumors, NPs as photothermal agents can accumulate in the tumor site and reduce the distribution in normal tissues, forming a temperature gradient between the tumor tissues and the normal tissues, which ensures that reduce the damage of tumor to surrounding normal tissue during PTT (Chen et al. 2022). At the same time, the use of photothermal agents can also reduce the power density and time of laser. Of course, to further improve the accumulation of nanoparticles at the tumor site,

targeting molecule-modified nanoprobes have been developed (-Xu et al. 2022). In addition, similar to some studies, our study found that the NPs prepared by us can also promote the maturation of DCs, which may have certain immunogenicity to improve the effect of immunotherapy (Zhao et al. 2013).

There are different views on the role of TLR7/8 agonists in the treatment for PDAC. An early study suggests that TLR7 is a principal modulator of the TME, driving neoplastic progression of human pancreatic cancer (Ochi et al. 2013). However, the recent study indicated that TLR7 expression is associated with the prognosis of human PDAC, and the high expression group has a better prognosis (Narayanan et al. 2019; Lanki et al. 2019). In recent years, a growing body of research has revealed R848 can remodel the tumor immune microenvironment and host responses in PDAC (Michaelis et al. 2019; Kim et al. 2019). Nowadays, ICB therapy has talent showing itself in immunotherapy, but the efficacy of ICB remains limited in PDAC (Li et al. 2021). The immunosuppressive microenvironment of PDAC is one of the main reasons for the poor response to ICB (Zhao et al. 2022). Our study of combination therapy can enhance the immunosuppressive microenvironment of PDAC, promote the maturation of DCs to enhance the efficacy of TAAs presentation, and stimulate T cell activation to induce an antitumor immune response. Currently, several studies have reported nanoparticle-based PTT with immune adjuvants and then binding to ICBs to induce a robust systemic anti-tumor immune response (Zhao et al. 2022). If $bTiO_2$@$mSiO_2$@Gd/R848 NPs combined with ICB for PDAC treatment may obtain more significant therapeutic effect. Furthermore, the incorporation of DOTA-Gd into the NPs enables the use of T_1-weighted MRI to monitor the progress of tumor treatment.

In conclusion, this work emphasizes the tremendous potential of combining immunotherapy and $bTiO_2$-based PTT as an excellent synergistic therapeutic method to treat PDAC while laying a foundation for the subsequent ICB combination therapy.

Acknowledgements
The authors thank Ningbo Cixi Institute of Biomedical Engineering for the help of synthesis and characterization of nanoparticles.

Author contributions
L.X., R.W. and J.N. contributed equally to this work. L.X. prepared nanoparticles and wrote the manuscript. R.W., J.N. and L.J. did a part of animal experiments. K.X., Y.Z., L.H. and C.C. conducted a statistical analysis of the study. L.W. and L.Z. analyzed the results of MRI. W.Z. analyzed the Figures of tissue staining. J.W. provided financial support, supervised the study, and reviewed the manuscript. All authors readand approved the final manuscript.

Funding
This study was supported by the National Natural Science Foundation of China (No.82172004), Ningbo Public welfare science and technology project (No.2021S181), Project of Ningbo Leading Medical & Health Discipline (No.2022-B15-A), Scientific research foundation of the national health commission—major science and technology project of medicine and health of zhejiang province (No.WKJ-ZJ-1912) and Ningbo Clinical Research Center for Medical Imaging (No.2022LYKFYB04).

Availability of data and materials
All data generated or analysed during this study are included in this published article.

Declarations

Ethics approval and consent to participate
For animal experiments, animal care and handling procedures were in agreement with the guidelines of the Regional Ethics Committee for Animal Experiments at Ningbo University.

Consent for publication
Not applicable.

Competing interests
The authors declare that they have no competing interests.

Received: 12 December 2023 Accepted: 24 May 2024
Published online: 04 June 2024

References

Balakrishnan PB, Sweeney EE, Ramanujam AS et al (2020) Photothermal therapies to improve immune checkpoint blockade for cancer. Int J Hyperthermia 37(3):34–49
Chen Y, Zhou F, Wang C et al (2022) Nanostructures as photothermal agents in tumor treatment. Molecules 28(1):277
Duan X, Chan C, Lin W (2019) Nanoparticle-mediated immunogenic cell death enables and potentiates cancer immunotherapy. Angew Chem Int Ed Engl 58(3):670–680
Gao S, Yang D, Fang Y et al (2019) Engineering nanoparticles for targeted remodeling of the tumor microenvironment to improve cancer immunotherapy. Theranostics 9(1):126–151
Guo C, Sun L, Cai H et al (2017) Gadolinium-labeled biodegradable dendron-hyaluronic acid hybrid and its subsequent application as a safe and efficient magnetic resonance imaging contrast agent. ACS Appl Mater Interfaces 9(28):23508–23519
Han HS, Choi KY (2021) Advances in nanomaterial-mediated photothermal cancer therapies: toward clinical applications. Biomedicines 9(3):305
Hou W, Yang B, Zhu H (2022) Nanoparticle-based therapeutic strategies for enhanced pancreatic ductal adenocarcinoma immunotherapy. Pharmaceutics 14(10):2033
Huang X, Lu Y, Guo M et al (2021) Recent strategies for nano-based PTT combined with immunotherapy: from a biomaterial point of view. Theranostics 11(15):7546–7569
Kim T, Lee N, Arifin DR et al (2017) In Vivo micro-CT imaging of human mesenchymal stem cells labeled with gold-poly-l-lysine nanocomplexes. Adv Funct Mater 27(3):1604213
Kim SY, Kim S, Kim JE et al (2019) Lyophilizable and multifaceted toll-like receptor 7/8 agonist-loaded nanoemulsion for the reprogramming of tumor microenvironments and enhanced cancer immunotherapy. ACS Nano 13(11):12671–12686
Lanki M, Seppänen H, Mustonen H et al (2019) Toll-like receptor 1 predicts favorable prognosis in pancreatic cancer. PLoS ONE 14(7):e0219245
Lee W, Suresh M (2022) Vaccine adjuvants to engage the cross-presentation pathway. Front Immunol 13:940047
Li W, Yang J, Luo L et al (2019) Targeting photodynamic and photothermal therapy to the endoplasmic reticulum enhances immunogenic cancer cell death. Nat Commun 10(1):3349
Li E, Huang X, Zhang G et al (2021) Combinational blockade of MET and PD-L1 improves pancreatic cancer immunotherapeutic efficacy. J Exp Clin Cancer Res 40(1):279
Liu L, Kshirsagar PG, Gautam SK et al (2022) Nanocarriers for pancreatic cancer imaging, treatments, and immunotherapies. Theranostics 12(3):1030–1060
Michaelis KA, Norgard MA, Zhu X et al (2019) The TLR7/8 agonist R848 remodels tumor and host responses to promote survival in pancreatic cancer. Nat Commun 10(1):4682
Muller M, Haghnejad V, Schaefer M et al (2022) The immune landscape of human pancreatic ductal carcinoma: key players, clinical implications, and challenges. Cancers (basel) 14(4):995
Narayanan JSS, Ray P, Hayashi T et al (2019) Irreversible electroporation combined with checkpoint blockade and TLR7 stimulation induces antitumor immunity in a murine pancreatic cancer model. Cancer Immunol Res 7(10):1714–1726
Neoptolemos JP, Kleeff J, Michl P et al (2018) Therapeutic developments in pancreatic cancer: current and future perspectives. Nat Rev Gastroenterol Hepatol 15(6):333–348
Nguyen HT, Tran KK, Sun B et al (2012) Activation of inflammasomes by tumor cell death mediated by gold nanoshells. Biomaterials 33(7):2197–2205
Ochi A, Graffeo CS, Zambirinis CP et al (2013) Toll-like receptor 7 regulates pancreatic carcinogenesis in mice and humans. J Clin Invest 122(11):4118–4129
Qi Z, Shi J, Zhang Z et al (2019) PEGylated graphene oxide-capped gold nanorods/silica nanoparticles as multifunctional drug delivery platform with enhanced near-infrared responsiveness. Mater Sci Eng C Mater Biol Appl 104:109889
Rawla P, Sunkara T, Gaduputi V (2019) Epidemiology of pancreatic cancer: global trends, etiology and risk factors. World J Oncol 10(1):10–27
Salvanou EA, Kolokithas-Ntoukas A, Liolios C et al (2022) Preliminary evaluation of iron oxide nanoparticles radiolabeled with 68Ga and 177Lu as potential theranostic agents. Nanomaterials (basel) 12(14):2490
Siegel RL, Miller KD, Fuchs HE et al (2022) (2022) Cancer statistics. CA Cancer J Clin 72(1):7–33
Sung H, Ferlay J, Siegel RL et al (2021) Global cancer statistics 2020: GLOBOCAN estimates of incidence and mortality worldwide for 36 cancers in 185 countries. CA Cancer J Clin 71(3):209–249
Vincent A, Herman J, Schulick R, Hruban RH, Goggins M (2011) Pancreatic cancer. Lancet 378:607–620
Wang S, Ren W, Wang J et al (2018) Black TiO_2-based nanoprobes for T_1-weighted MRI-guided photothermal therapy in CD133 high expressed pancreatic cancer stem-like cells. Biomater Sci 6(8):2209–2218
Wang M, Song J, Zhou F et al (2019) NIR-triggered phototherapy and immunotherapy via an antigen-capturing nanoplatform for metastatic cancer treatment. Adv Sci (weinh) 6(10):1802157
Wang M, Li Y, Wang M, Liu K, Hoover AR, Li M, Towner RA, Mukherjee P, Zhou F, Qu J, Chen WR (2022) Synergistic interventional photothermal therapy and immunotherapy using an iron oxide nanoplatform for the treatment of pancreatic cancer. Acta Biomater 138:453–462

Xu K, Jin L, Xu L et al (2022) IGF1 receptor-targeted black TiO_2 nanoprobes for MRI-guided synergetic photothermal-chemotherapy in drug resistant pancreatic tumor. J Nanobiotechnology 20(1):315
Zhang P, Chen D, Li L et al (2022) Charge reversal nano-systems for tumor therapy. J Nanobiotechnology 20(1):31
Zhang Y, Zhang Z (2020) The history and advances in cancer immunotherapy: understanding the characteristics of tumor-infiltrating immune cells and their therapeutic implications. Cell Mol Immunol 17(8):807–821
Zhang W, Zhang CC, Wang XY et al (2020) Light-responsive core-shell nanoplatform for bimodal imaging-guided photothermal therapy-primed cancer immunotherapy. ACS Appl Mater Interfaces 12(43):48420–48431
Zhao L, Seth A, Wibowo N et al (2013) Nanoparticle vaccines. Vaccine 32(3):327–337
Zhao Y, Liu X, Liu X et al (2022) Combination of phototherapy with immune checkpoint blockade: theory and practice in cancer. Front Immunol 13:955920
Zhou B, Song J, Wang M et al (2018a) BSA-bioinspired gold nanorods loaded with immunoadjuvant for the treatment of melanoma by combined photothermal therapy and immunotherapy. Nanoscale 10(46):21640–21647
Zhou F, Yang J, Zhang Y et al (2018b) Local phototherapy synergizes with immunoadjuvant for treatment of pancreatic cancer through induced immunogenic tumor vaccine. Clin Cancer Res 24(21):5335–5346

Publisher's Note